ACS OMEGA

http://pubs.acs.org/journal/acsodf

Article

Multifunctional Core@Satellite Magnetic Particles for Magnetoresistive Biosensors

Raffaele Campanile, Adriano Acunzo, Emanuela Scardapane, Antonio Minopoli, Veronica C. Martins, Rocco Di Girolamo, Susana Cardoso, Raffaele Velotta, Bartolomeo Della Ventura, and Vincenzo Iannotti*

Cite This: *ACS Omega* 2022, 7, 36543−36550

Read Online

ACCESS | Metrics & More | Article Recommendations | Supporting Information

ABSTRACT: Magnetoresistive (MR) biosensors combine distinctive features such as small size, low cost, good sensitivity, and propensity to be arrayed to perform multiplexed analysis. Magnetic nanoparticles (MNPs) are the ideal target for this platform, especially if modified not only to overcome their intrinsic tendency to aggregate and lack of stability but also to realize an interacting surface suitable for biofunctionalization without strongly losing their magnetic response. Here, we describe an MR biosensor in which commercial MNP clusters were coated with gold nanoparticles (AuNPs) and used to detect human IgG in water using an MR biochip that comprises six sensing regions, each one containing five U-shaped spin valve sensors. The isolated AuNPs (satellites) were stuck onto an aggregate of individual iron oxide crystals (core) so that the resulting core@satellite magnetic particles (CSMPs) could be functionalized by the photochemical immobilization technique—an easy procedure that leads to oriented antibodies immobilized upright onto gold. The morphological, optical, hydrodynamic, magnetic, and surface charge properties of CSMPs were compared with those exhibited by the commercial MNP clusters showing that the proposed coating procedure endows the MNP clusters with stability and ductility without being detrimental to magnetic properties. Eventually, the high-performance MR biosensor allowed us to detect human IgG in water with a detection limit of 13 pM (2 ng mL^{-1}). Given its portability, the biosensor described in this paper lends itself to a point-of-care device; moreover, the features of the MR biochip also make it suitable for multiplexed analysis.

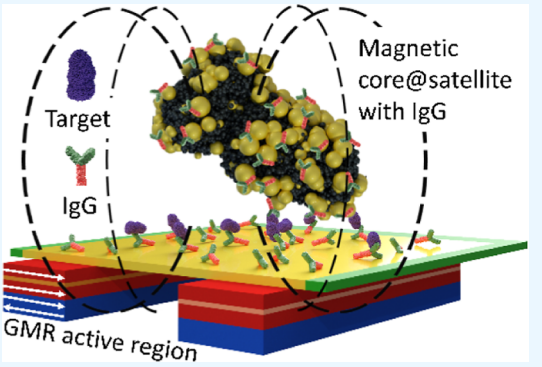

1. INTRODUCTION

In the past two decades, magnetic biosensors based on giant magnetoresistance (GMR) have drawn much attention for their simplicity in the nanofabrication process, very large functional area, and high linearity.[1−3] These sensors are compatible with CMOS integrated circuit technology, allowing them to be manufactured with an integrated electronic readout, produced in mass quantities (potentially at a low cost), and deployed in a disposable format for point-of-care (PoC) testing.[4,5] GMR spin-valve (SV)—consisting of two ferromagnetic layers separated by a nonferromagnetic layer—are usually preferred since they can operate at lower magnetic fields than those required for multilayer systems.[6] In this magnetoresistive (MR) biosensor, the stray field from each magnetic nanotag attached to the target produces a local change in the magnetic field, which, in turn, gives rise to a resistance change across the ferromagnetic layers. Thus, in order to increase the sensitivity of the biosensor, it is crucial that the magnetization of the nanotag be as large as possible.

Superparamagnetic nanoparticles (NPs) (approximately 20 nm for iron oxide NPs) have small magnetization in the field of 15−20 Oe—which is the intensity typically used to bias the sensors within the linear regime—and require progressively more sensitive sensors and measurement systems.[2] To circumvent such a limitation, magnetic clusters of NPs can be adopted since they show an enhanced and cooperative magnetic response that leads to an enhanced saturation magnetization and a reduced coercive field at low temperature.[7,8] Regardless of the size, magnetic surfaces require long biochemical procedures for their functionalization that can hardly be scaled up for industrial applications.[9] Such an issue can be effectively addressed by realizing the so-called core-satellite structures consisting of an iron oxide core with gold nanoparticles (AuNPs) adhered to its surface.[10] This can be considered an ideal coating[11] since gold is present like "spots" on the surface, making the functionalization to link bioreceptors easier[12]—relying on the gold surface chemistry

Received: July 14, 2022
Accepted: September 7, 2022
Published: October 4, 2022

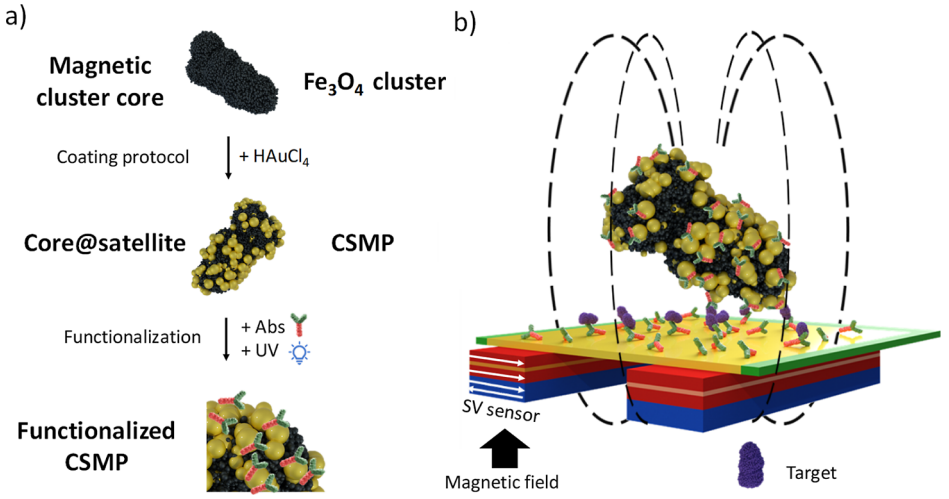

Figure 1. a) Commercial MNP (Fe_3O_4 MNP) clusters (diameter ≈ 250 nm) were coated with smaller AuNPs (diameter approximately 15−20 nm). The resulting CSMPs were functionalized by means of the PIT. (b) Schematic representation (not in scale) of the MR chip detection system. The gold pad over the SV sensor was functionalized by PIT as well. The Abs on the chip surface captured the targets in solution. Subsequently, functionalized CSMPs recognized the target, and a "sandwich" was formed. The fringe magnetic field due to CSMPs changed the magnetization of the free layer of the SV sensor, and the resulting flux difference was detected as a resistance change.

and biocompatibility[13]—while preserving the magnetic properties.

Here, we demonstrate that clusters of magnetic nanoparticles (MNPs) with AuNP satellites [core@satellite magnetic particles (CSMPs)] are effective tags for realizing high-sensitive GMR-based biosensor since the GMR signal is enhanced by the larger magnetic moment. To this end, we covered commercial MNPs made of Fe_3O_4 clusters (diameter ≈ 250 nm) with AuNPs of a smaller size (diameter approximately 15−20 nm) (Figure 1a). We found that the coating procedure conferred greater stability to the resulting CSMP clusters with no adverse effect on the magnetic properties. Thus, they could be used to produce the change of the magnetic field in close proximity of the MR biochip (Figure 1b). Moreover, given the excellent magnetic properties of CSMPs, the sensing scheme proposed in this work allowed to significantly increase the signal intensity, paving the way to further improvements in the limit of detection (LOD) and sensitivity even with other similar devices.

The lab-on-a-chip device was comprised of 6 sensing regions, each one containing 5 U-shaped SV sensors (30 SV sensor in total).[14] Each sensing region could be functionalized with a different antibody so that the biosensor was suitable for both signal redundancy and simultaneous monitoring of different antigens (6 targets at the same time) for high-throughput and/or multiplexed analysis. The biochip featured a unique and highly portable detection platform[15] specifically designed to be used as a PoC device.

The biochip surface was functionalized by the well-established photochemical immobilization technique (PIT).[16] This technique, based on a selective UV activation of antibodies (Abs), has proven to be an effective and competitive methodology since it is rapid and user-friendly and leads to strong (covalent) and conveniently oriented bonds of Abs on the sensor surfaces without affecting the intrinsic selectivity of the bioreceptors.[17−20] This is the first time that PIT is used in combination with a MR sensor and CSMPs and, as a proof of principle, we applied the biosensor to the detection of human IgG in water for which we achieved a LOD of 13 pM.

2. RESULTS AND DISCUSSION

2.1. CSMP Synthesis. The indirect gold coating proposed by Moraes Silva et al.[21] was modified by optimizing the concentrations of some reactants and by quickly cooling the final solution to avoid undesired aggregation. More specifically, the CSMPs were synthesized by dissolving the tetrachloroauric acid with positively charged PEGylated iron oxide composite particles. In a typical synthesis, 100 μL of magnetic particles [10 mg/mL] were added to a solution containing 15 mL of ultrapure water (Milli-Q) and 50 μL of a $HAuCl_4{\cdot}3H_2O$ (10 mg mL^{-1}). The solution was heated until 95 °C with vigorous stirring by using a mechanical motor stirrer (Heidolph RZR 50, Germany) rather than a standard magnetic stirrer to avoid nonspecific magnetic interaction. Once the temperature was reached, 1 mL of sodium citrate (100 mM) was added to induce acid reduction, as well as to produce the gold seeds, which anchored the PEG around the CSMPs. The citrate molecules acted both as a reducing agent and a capping agent, negatively charging the CSMPs and giving them the repulsive force that avoids the self-aggregation phenomena.[22]

The color changed 2 minutes after the second addition of 50 μL of a $HAuCl_4{\cdot}3H_2O$ at the same concentration. The color changed from an initial brown (Figure S1a) of the magnetic particles to a burgundy red (Figure S1b). The variation in the color was due to the growth of the gold around the gold seeds previously glued to the PEGylated MNPs. Eventually, the solution was cooled in ice by maintaining the same stirring speed.

When the room temperature was reached (about 10 minutes were required), CSMPs underwent 5 washing steps in which a magnet was used to remove the excess reagents and products dissolved in the supernatant. After the magnetic separation, the particles were resuspended in 10 mL of a buffer solution made of ultrapure water and Tween 20 (0.005%), the latter being a surfactant particularly used in the biosensing field to avoid nonspecific interactions. As a result of such a procedure, a colloidal solution of 10 mL of CSMPs (5×10^9 CSMPs mL^{-1}) was formed. It is worth mentioning that CSMPs in that buffer could stabilize and allow us to store them for several weeks.

https://doi.org/10.1021/acsomega.2c04442
ACS Omega 2022, 7, 36543−36550

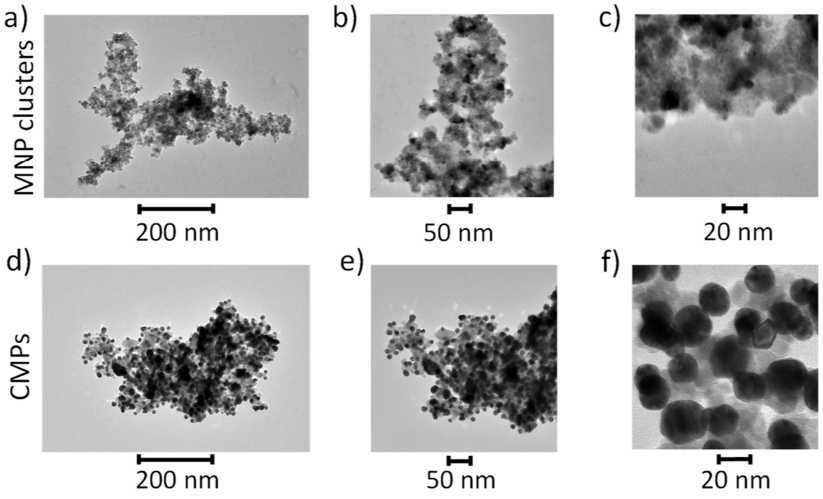

Figure 2. TEM micrographs at different magnification of (a−c) MNP clusters from the stock and (d−f) CSMPs. AuNPs with diameter approximately 15−20 nm are clearly visible on the surface of MNP clusters whose length scale is approximately 250 nm [panels (c,f)].

2.2. CSMPs Characterization. *2.2.1. Morphology.* Transmission electron microscopy (TEM) measurements allowed us to determine the morphology and shape of the particles. TEM micrographs were obtained using an FEI Tecnai G2 S-twin apparatus operating at 200 kV (LaB6 source). The particle powder samples were dispersed in water, and then a small quantity of the solution was added to the carbon-coated copper grid (200 mesh) and let evaporate. Figure 2 shows the micrographs of the bare MNP clusters as taken from the stock (panels a−c) and CSMPs (panels d−f). The irregular shape of the MNP cluster is quite common for clustered-type PEGylated iron oxide composite particles.[23,24] Nevertheless, since the detection signal relies upon the contribution of a large number of CSMPs that are close to the surface (Figure 1b), their uneven size distribution does not affect the device performance. For CSMPs, small AuNPs (diameter approximately 15−20 nm) are clearly visible [panel (f)] on the surfaces of the larger MNP clusters (diameter ≈ 250 nm) as a result of the coating protocol.

The presence of Au and Fe_3O_4 crystalline phases is also demonstrated by the X-ray diffraction (XRD) spectrum reported in Figure S2. XRD measurements were performed on dried NPs using nickel-filtered Cu Kα radiation (λ = 1.5418 Å) with a Philips automatic powder diffractometer.

2.2.2. DLS Measurements. In order to analyze the hydrodynamic behavior of CSMP suspension, dynamic light scattering (DLS) measurements were performed (Zetasizer Nano ZS instrument, Malvern Instruments Company). Figure 3a shows the size distributions of bare MNP clusters (black line) and CSMPs (red line) in ultrapure water. The size distribution for bare MNP clusters is unimodal, with the hydrodynamic diameter peaking at 260 nm, whereas the size distribution of the CSMPs is bimodal, with major and minor modes well separated from each other. For the major mode, the hydrodynamic diameter peaked at 350 nm, a value larger than that measured for bare MNP clusters as a result of the presence of the AuNPs on the surface. The secondary peak of CSMP size distribution is due to aggregates with a diameter larger than 1 μm and are byproducts of the gold coating process; however, their quick sedimentation allowed us to easily remove them from the solution.

2.2.3. Surface Charge Properties. Zeta potential measurements were carried out by the Zetasizer Nano ZS instrument

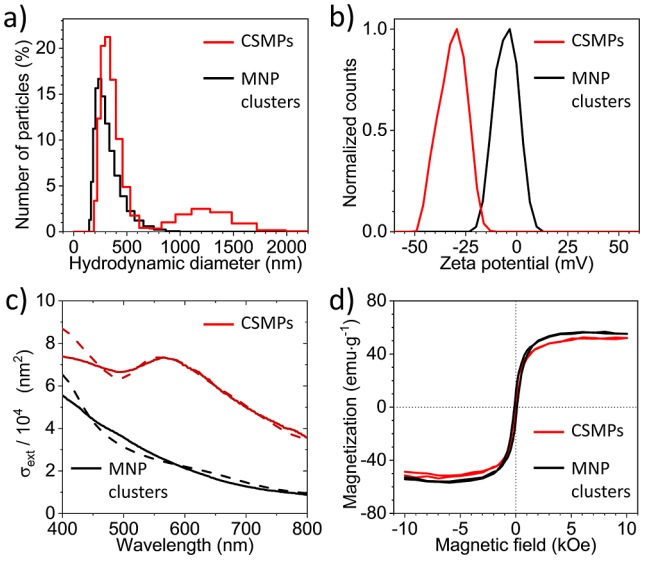

Figure 3. Black and red colors refer to the aqueous solutions of MNP clusters and CSMPs, respectively. (a) Size distributions retrieved from DLS measurements. (b) Zeta potential distributions. (c) Experimental (solid lines) and simulated (dashed lines) extinction spectra of MNP clusters and CSMPs, respectively. The extinction peak at 567 nm signaled the growth of AuNPs onto the MNP cluster surfaces after the coating process. (d) Hysteresis loops obtained by a VSM. Data are normalized to the total mass without subtracting the gold contribution.

(Malvern Instruments Company). The assessment of the zeta potential is crucial to gain insights into the stability and charge surface modifications of the colloidal solution of MNP clusters due to the gold coating.[25] As Figure 3b (black line) shows, the bare MNP clusters in an aqueous solution exhibit a zeta potential distribution peaked at around −3 mV. Such a low absolute value of the zeta potential is generally related to the instability of the colloidal solution.[25] On the contrary, the zeta potential distribution peak observed for CSMPs in water was about −30 mV (Figure 3b, red line), thus explaining the high stability of the colloidal solution, which was confirmed by the possibility that we had to use them several weeks after their synthesis. The negative shift of the Z-potential distribution is

https://doi.org/10.1021/acsomega.2c04442
ACS Omega 2022, 7, 36543−36550

consistent with the typical values of stable AuNP colloidal solutions in water.[26]

2.2.4. Optical response. The coating process induced a color change from brown (MNP clusters, Figure S1a) to burgundy red (CSMPs, Figure S1b). The presence of AuNPs on the surface of the MNP clusters was also confirmed by the spectroscopic measurements (Jenway 6715 UV/VIS spectrophotometer). The results are shown in Figure 3c, in which the continuous lines refer to the experimental extinction spectra of MNP clusters (black) and CSMPs (red), respectively. While the extinction spectra of the MNP clusters do not show any extinction peak, the spectra of the CSMPs show a prominent resonance at 567 nm as a result of the presence of AuNPs. It is worth to mention that CSMPs solution was cleaned by magnetic separation several times (Section 2.1) to ensure that free AuNPs in solution were removed, and only AuNPs grafted to MNP clusters contributed to the spectrum shown in Figure 3c.

In order to corroborate the experimental results, we simulated the optical response of an aqueous solution containing core@satellite particles by the finite-difference time-domain method,[27] which we recently used to simulate the optical behavior of AuNPs grafted to a virus.[28] A detailed description of the simulation workspace is reported in Supporting Information (Figure S3a), whereas the results are shown in terms of extinction cross-section (σ_{ext}) in Figure 3c for MNP clusters (dashed black) and CSMPs (dashed red), respectively.

The excellent agreement between theory and experiment was achieved by considering MNP clusters as prolate spheroids (axes lengths 250 nm × 130 nm × 130 nm). The dimensions were optimized against the experimental MNP cluster extinction spectra by keeping constant the major axis (250 nm), a value provided by the seller company but also confirmed by DLS measurements. The optimization procedure and the dependence of the extinction spectra on the spheroid dimensions are discussed in the Supporting Information (Section S3, Figure S3c). It is worth noticing that the extinction spectrum of MNP clusters is quite sensitive to the particle geometry; for instance, a sphere with a comparable dimension yielded a significantly different spectrum (Figure S3b).

The CSMPs were simulated with AuNPs with a 15 nm diameter—an average value resulting from the analysis of the TEM images— and the excellent agreement shown in Figure 3c was achieved with a degree of covering of 85% (Figure S3d). This result corroborates the claim that CSMPs are made of MNP clusters coated by AuNPs with a high degree of covering.

2.2.5. Magnetic Properties. The magnetic properties of both MNP clusters and CSMPs were assessed with a vibrating-sample magnetometer (VSM) (DSM 880, Microsense). The hysteresis loops (Figure 3d) were measured at 300 K, and the saturation magnetizations turned out to be 55 and 51 emu g^{-1} for MNP clusters and CSMPs, respectively. The weakening of the magnetic properties of MNPs when coated with gold is a well-known phenomena[29,30] that arises from the diamagnetic nature of gold; thus, an unavoidable trade-off between the gold coating and high magnetic moment has to be reached if MNPs are to be used in a biological environment. In our case, we were able to synthesize CSMPs for which the saturation magnetization was only reduced by 10%. The fragmented rather than uniform gold coating is one of the main reasons that make CSMPs a better choice than fully coated MNP since, in this way, there is no "heavy" diamagnetic layer, and the initial magnetic properties are essentially kept. In the biosensing experiment we carried out, the applied magnetic field was 35 Oe, a value that falls within the linear range of the hysteresis curve.

2.3. Biosensing Results. *2.3.1. Detection of Human IgG in Water.* The dose–response curve was obtained by measuring the GMR signal ($\Delta V \cdot V^{-1}$), as described in Section 4.5, at several IgG concentrations. The results are reported in

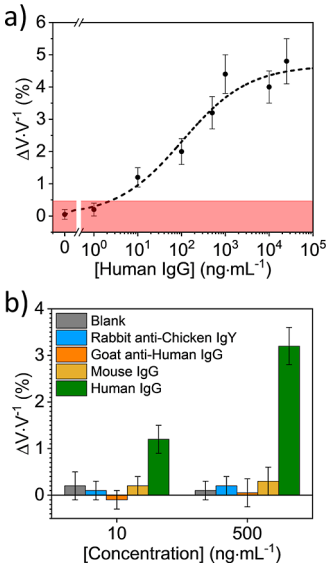

Figure 4. (a) Dose–response curve. Experimental data were fitted to eq 1. Each data point was duplicated with a different biochip. (b) Sensor specificity. The signal obtained with Abs other than human IgG is compatible with blank.

Figure 4a together with the best fit of the experimental data provided by the three-parameters Hill's equation[31]

$$\frac{\Delta V}{V} = \frac{a[x]^n}{[x]^n + k^n} \quad (1)$$

that yielded $a = 4.7 \pm 0.5$, $k = 105 \pm 70$ ng mL^{-1}, n=0.6 ± 0.1 (negatively cooperative binding), with R-squared equal to 0.98. The dose-response curve exhibits signal saturation at concentrations higher than 1 μg mL^{-1}, thus showing that the MR biochip, in combination with CSMPs, is able to provide a quantitative measurement over three decades. The error bars originate from biological variability, and each data point of the dose–response curve is the result of the average of over 30 values from 2 different chips (one duplicate), each of them with 15 sensing surfaces. Since each experiment was performed with a different biochip, the uncertainties reported in Figure 4a include the chip-to-chip difference arising from the fabrication, thereby confirming the robustness of the biosensor against the differences in kit components of the biosensor. Since the experiments were carried out on different days, the goodness of fit reported in Figure 4a also demonstrates satisfactory day-to-day repeatability.

The LOD assessed by means of 3 standard deviation (red shaded area Figure 4a) turned up to be 2 ng mL^{-1} (13 pM). It is worth pointing out that the GMR signal at a concentration in the order of 1 ng mL^{-1} is approximately 3 × 10^{-3}, a value

https://doi.org/10.1021/acsomega.2c04442
ACS Omega 2022, 7, 36543−36550

significantly larger than that obtained with a similar experimental layout but with "ordinary" magnetic beads.[32] The relatively large GMR signal entailed by CSMPs is also comparable to that achieved by other groups who obtained approximately 500 ppm at 250 pg/mL for both human IL6[33] and Human NT-ProBNP.[34] However, compared to our detection scheme (Figure 1), the latter approach required an additional step since the MNPs tethered the secondary Abs rather than the analyte.

2.3.2. Specificity Assay. The specificity of the immunosensor was proved by testing the detection of compounds similar to human IgG by using the same experimental procedure. Thus, we measured the response of the sensor to mouse IgG, goat antihuman IgG, and rabbit antichicken IGY with the same experimental procedure used for the detection of human IgG but at a higher (500 ng mL^{-1}, i.e., 3.3 nM), as well as lower (10 ng mL^{-1}, i.e., 67 pM) concentration so as to circumvent the occurrence of a possible hook effect. Remarkably, Figure 4b shows that the signals obtained with analytes other than human IgG were in the same range as the control signal and significantly different from what was obtained for the human IgG at the same concentration.

3. CONCLUSIONS

We report the use of CSMPs as a versatile substrate for efficient detection by a magneto resistive chip. The CSMPs were realized by inducing gold self-assembling onto a cluster of MNP so that they could exhibit strong magnetization and high stability in a colloidal solution. The presence of AuNPs on their surface allowed us to exploit a gold surface functionalization technique (PIT) to tether oriented Abs onto CSMPs, making them immunoreactive and capable of inducing a strong response by a magnetic transducer.

In fact, we used CSMPs in a biosensing procedure relying on an MR biochip to realize a device whose sensitivity is enhanced by the large magnetic moment of CSMP that is kept even when they are decorated by AuNPs. As a proof of concept, we detected human IgG in an interesting range for biomedical applications (1−1000 ng mL^{-1}) with a LOD of 2 ng mL^{-1} (13 pM). The target (human IgG) was captured by an MR chip functionalized with antihuman IgG, and then CSMPs (functionalized with anti-human IgG) were used to form a "sandwich." The close distance between the CSMPs and the chip surface induced a magnetization change of the SV sensor that, in turn, yielded a detectable resistance variation (GMR effect).

As for all the immunoassays, the specificity was very high, and essentially no signal could be detected with proteins other than human IgGs. Since the detection principle relies on the formation of a sandwich, we can safely expect that 13 pM is still a reachable LOD even when smaller analytes are targeted. This means that with an analyte of a few hundreds of Daltons, our biosensor may reach an LOD of a few pg mL^{-1}. Moreover, thanks to the chip geometry and detection scheme, we point out that the proposed biosensor inherently lends itself to multiplexed analysis with up to six different analytes.

4. EXPERIMENTAL SECTION

4.1. Reagents and Materials. The ultrapure water used in the preparation of any solution was Milli-Q (resistivity 24 MΩ cm). Tetrachloroauric acid ($HAuCl_4 \cdot 3H_2O$), sodium citrate ($Na_3C_6H_5O_7$), and polysorbate 20 (Tween 20, $C_{26}H_{50}O_{10}$) were purchased by Sigma-Aldrich. All the Abs used for this study were purchased from ImmunoReagents. Bovine serum albumin (BSA) was purchased from Pierce. The PEGylated iron oxide composite particles were purchased from MicroMod (product name nanomag-D, product code 09-54-252). They have a core−shell-like structure with a core of magnetite and a dextran shell. The magnetite core consists of aggregates of individual iron oxide (magnetite) crystals with diameters of 5−15 nm. Their dextran surface has been modified with PEG 300 in order to limit the unspecific protein from binding on the particle surface.

4.2. GMR Sensor Fabrication and Cleaning. The MR biochip contains 6 sensing regions enclosed in a gold squared frame (300 × 300 μm^2), each one containing 5 U-shaped SV sensors (80 × 2.6 μm^2) coated with a gold pad (35 × 13 μm^2) for a total of 30 SV sensors (Figure S4). The 6 sensitive regions are arranged in two parallel rows, three on the left side and three on the right side. The several microfabrication steps involved in the manufacturing of the SV biochips have been previously described.[35] Briefly, the SV materials were deposited by an ion beam in a Nordiko 3000 tool[36] on a 150 mm diameter silicon wafer, passivated with 100 nm of alumina (Al_2O_3 deposited by sputtering from a ceramic target, with a power of 200 W, 4.5 mTorr). The SV multilayer structure was the following: Ta 20 nm/NiFe 25 nm/CoFe 28 nm/Cu 26 nm/CoFe 24 nm/MnIr 70 nm/Ta 50 nm. The sensors were patterned using direct write laser lithography (Heidelberg DWL 2.0, diode laser wavelength 405 nm), transferred to the substrate by ion milling etching [Nordiko 3000, using an Ar^+ beam with 29 mA (92 $\mu A/cm^2$), acceleration V^+ = 500 V, extraction V^- = 200 V, at a pressure $p = 2.4 \times 10^{-4}$ Torr and beam-to-surface angle = 70° for 400 s], and protected with a 350 nm thick Si_3N_4 passivation layer deposited by PECVD in an Oxford tool (SiH_4 = 20 sccm, N_2 = 20 sccm, N_2O = 980 sccm, at a pressure of 1 Torr and 300 °C), where the gold pads deposited were then defined over the sensors. Before every biosensing experiment, the chips underwent a cleaning process. The sensing region was rinsed multiple times with ultrapure water and isopropyl alcohol. Once dried with an air compressor, they were exposed to an ultraviolet light/ozone plasma for 15 min at 28 mW cm^{-2} at 5 mm separation from the UV lamp inside a UVO cleaner machine from Jelight (Irvine, CA, USA). The biochips could be recycled several times using the abovementioned procedure.

4.3. Functionalization Protocol. In this experiment, half of the sensors were functionalized with goat antihuman IgG (in order to detect human IgG), and the remaining half was functionalized with donkey antisheep IgG (negative control). To the best of our knowledge, this is the first time that the PIT[16] was employed in combination with MR sensors. The PIT is a powerful and fast methodology whose effectiveness has already been confirmed in several biosensing applications.[17,18,37,38] It is based on selective UV activation of Abs that leads to a strong covalent binding to noble metal surfaces that improve the detection efficiency of the immunosensor, orienting the Abs with the fragment antigen-binding site (Fab) exposed to the solvent. The functionalization procedure via the PIT involved the following steps: (1) a quartz cuvette containing 1 mL of Abs dissolved in ultrapure water (25 μg mL^{-1}) was irradiated by UV light lamp (Trylight) for 30 s (Figure S5), which is the optimal irradiation time for PIT; (2) immediately after irradiation, the solution was manually spotted on the chip surface, one droplet covering the 3

https://doi.org/10.1021/acsomega.2c04442
ACS Omega 2022, 7, 36543−36550

sensing regions (goat antihuman IgG for sensors from 1 to 15, donkey antisheep IgG for sensors from 16 to 30); (3) the substrates were left at room temperature inside a humid chamber for 10 min after which (4) the unbound Abs were washed with ultrapure water.

Once the unbound Abs were removed, 30 μL of a solution of 5% BSA was deposited on the surface of the chip in order to fill any unoccupied area left after functionalization in order to minimize nonspecific contributions. The chip was incubated for 1 h, after which it was washed with ultrapure water. Using a different protocol, the CSMPs were also functionalized by the PIT. First, a volume of 2 mL of the solution resulting from the above-mentioned coating protocol was concentrated in a volume of 100 μL by means of magnetic separation. Separately, a 100 μL of Abs solution (10 μg mL^{-1}) was irradiated by UV light for 30 s and later was added in 10 spikes (5 μL each) to the CSMP solution. The functionalized CSMPs were gently stirred for 10 min. As a final step, the CSMPs were magnetically separated from the solution in order to remove the Abs in excess and resuspended in 10 μL of water to be conveyed into the microfluidic circuit that crosses the sensors.

4.4. Biochip Setup. The biochip detection platform was fabricated as previously described.[39] Briefly, the system is divided into five main sections: the chip insertion site, copper coil for the magnetic drive, battery, USB connector, and box containing the detection electronic circuit (Figure S6). The removable microfluidics circuit, made of polydimethylsiloxane (PDMS), is placed above the chip with the possibility to be connected to any pumping system. The metal box has the purpose of shielding the circuits from external signals that could cause interference with the measurement process.

The platform was built to be an autonomous, versatile, and secure system able to perform real-time signal processing using standard communication technologies. To this end, the detection electronic circuit is composed of three main modules: a sensing and processing module (SPM), an autonomous communication module (ACoM), and an analyzer module (AnM). Thanks to SPM and ACoM modules, the platform can be directly connected to a PC and fully controlled using the specially designed graphic user interface (GUI) (Figure S7). The SPM is equipped with a sensor interface block that performs multiplexing and conditioning of the signal of each sensor.[39] In particular, the electric current generator that drives and biases the circuit interrogates each biochip sensing site independently.

The ACoM module contains a data transfer manager and a set of standard interfaces for wire and wireless communication. The transfer manager is responsible for communicating data and commands from and to the SPM and the AnM. ACoM controls the state of the battery and recharges it whenever necessary, draining the energy from external power suppliers or communication buses (e.g., USB connection to the PC). Both SPM and ACoM were implemented onto two printed circuit boards of equal size (32 cm^2) and stacked inside a steel noise shielding enclosure. AnM is the module that has full control over the embedded system. Taking advantage of the AnM module, the acquired signals are processed in real time and transmitted to a digital analyzer that enables the user to control and follow the experiment. AnM is also responsible for the capability of the platform to connect to the internet, allowing communication to remote databases by using WebServices.

All the electronic circuitry for addressing, driving, and reading out signals from SV or magnetic tunnel junctions sensors is implemented using off-the-shelf components. The developed platform is portable (15 cm × 13 cm × 4 cm) and capable of operating autonomously for nearly 8 h. The battery can be recharged by the PC using the same connection used to operate the platform.

4.5. Experimental Procedure. 30 μL of a solution containing the antigen to be detected at fixed concentrations was spotted on the sensor, whose surface was functionalized with Abs and blocked with BSA, as described in Section 4.3. After being incubated for 1 h, the chip was washed with ultrapure water and inserted in the specifically designed MR biochip platform (Section 4.4). A U-shaped PDMS microfluidic channel 800 × 300 μm^2 (width × height) was placed over the chip to transport the functionalized CSMPs over the sensing area.

The measurements started with a voltage baseline acquisition of around 5−10 min. When the signal was stable, the CSMP solution, functionalized and concentrated, as described in Section 4.3, was conveyed to the microfluidic circuit by means of a syringe pump (New Era Pump systems) at a flow rate of 50 μL min^{-1}(Figure S8). The flux was stopped when the solution completely filled the channel, meaning the CSMPs were over the sensing area. After 10 minutes, once the voltage signal of the sensors was saturated, the unbound CSMPs were washed out with water at a flow rate of 150 μL min^{-1} for 5 min. If there were differences between the initial baseline voltage ($V_{baseline}$) and the final voltage after the washing ($V_{washing}$), a binding signal ΔV was obtained.

The binding voltage difference ($V_{baseline} - V_{washing}$) was measured both for the detection (ΔV^p) and the negative (ΔV^n) control sensors (Figure 5). Then, the mean value of the

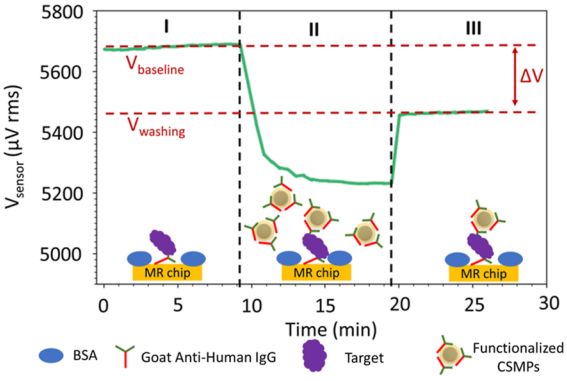

Figure 5. Typical dynamic response of the MR biosensor (sensorgram). The *y*-axis shows the potential difference across the chip, and the *x*-axis shows the time interval. The green line represents the response of the sensor in each of the following steps: (I) voltage baseline acquisition (flow rate 50 μL min^{-1}), (II) CSMPs interacting with the sensor (static), and (III) washing step (flow rate 150 μL min^{-1}).

voltage variation for the negative control sensors ΔV^n was subtracted from ΔV^p for each positive sensor, and finally, each ΔV was divided by the baseline voltage value of each sensor. The sensors were biased with a 1 mA CD current, and the magnetic drive was set to 35 Oe DC. An additional time-varying magnetic field was employed with 13.5 Oe rms AC at 211 Hz.

For each sensor, a transfer curve, as the one shown in Figure S9, was acquired. The transfer curve shows the resistance of the chip versus the applied DC magnetic field from −120 to

https://doi.org/10.1021/acsomega.2c04442
ACS Omega 2022, 7, 36543−36550

120 Oe. The magnetic drive field was chosen so as to fix the working point in the linear region of the transfer curve. The data were sequentially recorded at a bandwidth of 4 Hz and 2 samples per sensor.

■ ASSOCIATED CONTENT

Supporting Information

The Supporting Information is available free of charge at https://pubs.acs.org/doi/10.1021/acsomega.2c04442.

Color of the MNP clusters solution before and after the gold coating (Figure S1); XRD spectrum of CSMPs (Figure S2); details about the numerical simulations of the optical response (Figure S3); description of the MR biochip (Figure S4); functionalization procedure of the substrate and CSMPs (Figure S5); biochip detection platform (Figure S6);p rint screen of the GUI (Figure S7); picture of the experimental set-up (Figure S8); example of a transfer curve of a SV sensor (Figure S9) (PDF)

■ AUTHOR INFORMATION

Corresponding Author

Vincenzo Iannotti − *Department of Physics "E. Pancini", University of Naples Federico II, 80126 Naples, Italy; CNR—SPIN (Institute for Superconductors, Oxides and Other Innovative Materials and Devices), 80125 Naples, Italy;* orcid.org/0000-0001-7229-5045; Email: viannotti@unina.it

Authors

Raffaele Campanile − *Department of Physics "E. Pancini", University of Naples Federico II, 80126 Naples, Italy;* orcid.org/0000-0002-0753-916X

Adriano Acunzo − *Department of Physics "E. Pancini", University of Naples Federico II, 80126 Naples, Italy;* orcid.org/0000-0003-3219-4623

Emanuela Scardapane − *Department of Physics "E. Pancini", University of Naples Federico II, 80126 Naples, Italy;* orcid.org/0000-0003-3667-8166

Antonio Minopoli − *Department of Physics "E. Pancini", University of Naples Federico II, 80126 Naples, Italy*

Veronica C. Martins − *INESC—Microsistemas e Nanotecnologias, 1000-049 Lisbon, Portugal*

Rocco Di Girolamo − *Department of Chemistry, University of Naples Federico II, 80126 Naples, Italy;* orcid.org/0000-0001-8815-2997

Susana Cardoso − *INESC—Microsistemas e Nanotecnologias, 1000-049 Lisbon, Portugal; Instituto Superior Tecnico (IST), Universidade de Lisboa, 1649-004 Lisboa, Portugal;* orcid.org/0000-0001-6913-6529

Raffaele Velotta − *Department of Physics "E. Pancini", University of Naples Federico II, 80126 Naples, Italy;* orcid.org/0000-0003-1077-8353

Bartolomeo Della Ventura − *Department of Physics "E. Pancini", University of Naples Federico II, 80126 Naples, Italy;* orcid.org/0000-0003-2920-6187

Complete contact information is available at: https://pubs.acs.org/10.1021/acsomega.2c04442

Author Contributions

R.C., R.V., V.I., and S.C. conceived the project. R.C. carried out the experiments and collected the data under V.C.M., B.D.V., and S.C.'s supervision and administration. A.A. and A.M. worked out the numerical simulations. R.C., E.S., B.D.V., V.I., and R.V. performed the data interpretation. R.C. and A.M. realized the figures. R.D.G. carried out the TEM microscopy. R.V. and B.D.V. dealt with funding acquisition. R.C. wrote the manuscript. V.I. and R.V. revised the manuscript.

Notes

The authors declare no competing financial interest.

■ ACKNOWLEDGMENTS

INESC-MN wish to acknowledge the Fundação para a Ciência e a Tecnologia for funding the Research Unit INESC MN (UID/05367/2020) through pluriannual BASE and PROGRAMATICO financing. The work was partially supported by the Moore4Medical project funded by the ECSEL joint undertaking under grant number H2020-ECSEL-2019-IA-876190 and the University of Naples Federico II under the scheme FRA-LineaB_2021 (CUP E65F21000580005).

■ REFERENCES

(1) Baselt, D. R.; Lee, G. U.; Natesan, M.; Metzger, S. W.; Sheehan, P. E.; Colton, R. J. A Biosensor Based on Magnetoresistance Technology. *Biosens. Bioelectron.* **1998**, *13*, 731−739.

(2) Graham, D. L.; Ferreira, H. A.; Freitas, P. P. Magnetoresistive-Based Biosensors and Biochips. *Trends Biotechnol.* **2004**, *22*, 455−462.

(3) Lim, B.; Mahfoud, M.; Das, P. T.; Jeon, T.; Jeon, C.; Kim, M.; Nguyen, T.-K.; Tran, Q.-H.; Terki, F.; Kim, C. Advances and Key Technologies in Magnetoresistive Sensors with High Thermal Stabilities and Low Field Detectivities. *APL Mater.* **2022**, *10*, 051108.

(4) Hall, D. A.; Gaster, R. S.; Makinwa, K. A. A.; Wang, S. X.; Murmann, B. A. A 256 Pixel Magnetoresistive Biosensor Microarray in 0.18 μm CMOS. *IEEE J. Solid-State Circuits* **2013**, *48*, 1290−1301.

(5) Wu, K.; Tonini, D.; Liang, S.; Saha, R.; Chugh, V. K.; Wang, J. P. Giant Magnetoresistance Biosensors in Biomedical Applications. *ACS Appl. Mater. Interfaces* **2022**, *14*, 9945−9969.

(6) Cardoso de Freitas, S.; Knudde, S.; Cardoso, F. A.; Freitas, P. P.Spin Valve and Tunnel Magnetoresistance Sensors. In *Magnetic Nanoparticles in Biosensing and Medicine*; Darton, N. J., Ionescu, A., Llandro, J., Eds.; Cambridge University Press, 2019; pp 181−206.

(7) Kostopoulou, A.; Brintakis, K.; Vasilakaki, M.; Trohidou, K. N.; Douvalis, A. P.; Lascialfari, A.; Manna, L.; Lappas, A. Assembly-Mediated Interplay of Dipolar Interactions and Surface Spin Disorder in Colloidal Maghemite Nanoclusters. *Nanoscale* **2014**, *6*, 3764−3776.

(8) Lartigue, L.; Hugounenq, P.; Alloyeau, D.; Clarke, S. P.; Lévy, M.; Bacri, J. C.; Bazzi, R.; Brougham, D. F.; Wilhelm, C.; Gazeau, F. Cooperative Organization in Iron Oxide Multi-Core Nanoparticles Potentiates Their Efficiency as Heating Mediators and MRI Contrast Agents. *ACS Nano* **2012**, *6*, 10935−10949.

(9) Tripathy, A.; Nine, M. J.; Silva, F. S. Biosensing Platform on Ferrite Magnetic Nanoparticles: Synthesis, Functionalization, Mechanism and Applications. *Adv. Colloid Interface Sci.* **2021**, *290*, 102380.

(10) Chen, H.; Hu, H.; Tao, C.; Clauson, R. M.; Moncion, I.; Luan, X.; Hwang, S.; Sough, A.; Sansanaphongpricha, K.; Liao, J.; et al. Self-Assembled Au@Fe Core/Satellite Magnetic Nanoparticles for Versatile Biomolecule Functionalization. *ACS Appl. Mater. Interfaces* **2019**, *11*, 23858−23869.

(11) Gessner, I.; Park, J.; Lin, H.; Lee, H.; Weissleder, R. Magnetic Gold Nanoparticles with Idealized Coating for Enhanced Point-Of-Care Sensing. *Adv. Healthcare Mater.* **2022**, *11*, 2102035.

(12) Chaudhary, A.; Khan, S.; Gupta, A.; Nandi, C. K. Effect of Surface Chemistry and Morphology of Gold Nanoparticle on the Structure and Activity of Common Blood Proteins. *New J. Chem.* **2016**, *40*, 4879−4883.

(13) Zhang, J.; Mou, L.; Jiang, X. Surface Chemistry of Gold Nanoparticles for Health-Related Applications. *Chem. Sci.* **2020**, *11*, 923−936.

(14) Martins, V. C.; Germano, J.; Cardoso, F. A.; Loureiro, J.; Cardoso, S.; Sousa, L.; Piedade, M.; Fonseca, L. P.; Freitas, P. P. Challenges and Trends in the Development of a Magnetoresistive Biochip Portable Platform. *J. Magn. Magn. Mater.* **2010**, *322*, 1655−1663.
(15) Germano, J.; Costa, T.; Cardoso, F. A.; Amaral, J.; Cardoso, S.; Freitas, P. P.; Piedade, M. S.Electronic Platforms and Signal Processing for Magnetoresistive-Based Biochips. In *Handbook of Biochips*; Sawan, M., Ed.; Springer: New York, NY, 2017; pp 1−39.
(16) Della Ventura, B.; Banchelli, M.; Funari, R.; Illiano, A.; De Angelis, M.; Taroni, P.; Amoresano, A.; Matteini, P.; Velotta, R. Biosensor Surface Functionalization by a Simple Photochemical Immobilization of Antibodies: Experimental Characterization by Mass Spectrometry and Surface Enhanced Raman Spectroscopy. *Analyst* **2019**, *144*, 6871−6880.
(17) Cimafonte, M.; Fulgione, A.; Gaglione, R.; Papaianni, M.; Capparelli, R.; Arciello, A.; Bolletti Censi, S.; Borriello, G.; Velotta, R.; Della Ventura, B. Screen Printed Based Impedimetric Immunosensor for Rapid Detection of Escherichia Coli in Drinking Water. *Sensors* **2020**, *20*, 274.
(18) Ventura, B.; Cennamo, M.; Minopoli, A.; Campanile, R.; Censi, S.; Terracciano, D.; Portella, G.; Velotta, R. Colorimetric Test for Fast Detection of SARS-CoV-2 in Nasal and Throat Swabs. *ACS Sens.* **2020**, *5*, 3043−3048.
(19) Minopoli, A.; Della Ventura, B.; Lenyk, B.; Gentile, F.; Tanner, J. A.; Offenhäusser, A.; Mayer, D.; Velotta, R. Ultrasensitive Antibody-Aptamer Plasmonic Biosensor for Malaria Biomarker Detection in Whole Blood. *Nat. Commun.* **2020**, *11*, 6134.
(20) Minopoli, A.; Della Ventura, B.; Campanile, R.; Tanner, J. A.; Offenhäusser, A.; Mayer, D.; Velotta, R. Randomly Positioned Gold Nanoparticles as Fluorescence Enhancers in Apta-Immunosensor for Malaria Test. *Microchim. Acta* **2021**, *188*, 88.
(21) Moraes Silva, S.; Tavallaie, R.; Sandiford, L.; Tilley, R. D.; Gooding, J. J. Gold Coated Magnetic Nanoparticles: From Preparation to Surface Modification for Analytical and Biomedical Applications. *Chem. Commun.* **2016**, *52*, 7528−7540.
(22) El-Nour, K. M. A.; Salam, E. T. A.; Soliman, H. M.; Orabi, A. S. Gold Nanoparticles as a Direct and Rapid Sensor for Sensitive Analytical Detection of Biogenic Amines. *Nanoscale Res. Lett.* **2017**, *12*, 231.
(23) Tóth, I. Y.; Nesztor, D.; Novák, L.; Illés, E.; Szekeres, M.; Szabó, T.; Tombácz, E. Clustering of Carboxylated Magnetite Nanoparticles through Polyethylenimine: Covalent versus Electrostatic Approach. *J. Magn. Magn. Mater.* **2017**, *427*, 280−288.
(24) Saikia, K.; Sen, D.; Mazumder, S.; Deb, P. Reassembling Nanometric Magnetic Subunits into Secondary Nanostructures with Controlled Interparticle Spacing. *RSC Adv.* **2015**, *5*, 694−705.
(25) Bhattacharjee, S. Review Article DLS and Zeta Potential − What They Are and What They Are Not. *J. Controlled Release* **2016**, *235*, 337−351.
(26) Tantra, R.; Schulze, P.; Quincey, P. Particuology Effect of Nanoparticle Concentration on Zeta-Potential Measurement Results and Reproducibility. *Particuology* **2010**, *8*, 279−285.
(27) Kane Yee, Y. Numerical Solution of Initial Boundary Value Problems Involving Maxwell's Equations in Isotropic Media. *IEEE Trans. Antennas Propag.* **1966**, *14*, 302−307.
(28) Minopoli, A.; Scardapane, E.; Acunzo, A.; Campanile, R.; Della Ventura, B.; Velotta, R. Analysis of the Optical Response of a SARS-CoV-2-Directed Colorimetric Immunosensor. *AIP Adv.* **2021**, *11*, 065319.
(29) Zhou, H.; Lee, J.; Park, T. J.; Lee, S. J.; Park, J. Y.; Lee, J. Ultrasensitive DNA Monitoring by Au-Fe 3O 4 Nanocomplex. *Sens. Actuators, B* **2012**, *163*, 224−232.
(30) Goon, I. Y.; Lai, L. M. H.; Lim, M.; Munroe, P.; Gooding, J. J.; Amal, R. Fabrication and Dispersion of Gold-Shell-Protected Magnetite Nanoparticles: Systematic Control Using Polyethyleneimine. *Chem. Mater.* **2009**, *21*, 673−681.
(31) Goutelle, S.; Maurin, M.; Rougier, F.; Barbaut, X.; Bourguignon, L.; Ducher, M.; Maire, P. The Hill Equation: A Review of Its Capabilities in Pharmacological Modelling. *Fundam. Clin. Pharmacol.* **2008**, *22*, 633−648.
(32) Devkota, J.; Kokkinis, G.; Berris, T.; Jamalieh, M.; Cardoso, S.; Cardoso, F.; Srikanth, H.; Phan, M. H.; Giouroudi, I. A Novel Approach for Detection and Quantification of Magnetic Nanomarkers Using a Spin Valve GMR-Integrated Microfluidic Sensor. *RSC Adv.* **2015**, *5*, 51169−51175.
(33) Klein, T.; Wang, W.; Yu, L.; Wu, K.; Boylan, K. L. M.; Vogel, R. I.; Skubitz, A. P. N.; Wang, J. P. Development of a Multiplexed Giant Magnetoresistive Biosensor Array Prototype to Quantify Ovarian Cancer Biomarkers. *Biosens. Bioelectron.* **2019**, *126*, 301−307.
(34) Wang, W.; Klein, T.; Collins, J.Giant Magnetoresistive Based Handheld System for Rapid Detection of Human NT-ProBNP. *Design of Medical Devices Conference*; American Society of Mechanical Engineers, 2019.
(35) Martins, V. C.; Cardoso, F. A.; Germano, J.; Cardoso, S.; Sousa, L.; Piedade, M.; Freitas, P. P.; Fonseca, L. P. Femtomolar Limit of Detection with a Magnetoresistive Biochip. *Biosens. Bioelectron.* **2009**, *24*, 2690−2695.
(36) Gehanno, V.; Freitas, P. P.; Veloso, A.; Ferrira, J.; Almeida, B.; Soasa, B.; Kling, A.; Soares, M. F.; da Silva, M. F. Ion Beam Deposition of Mn-Ir Spin Valves. *IEEE Trans. Magn.* **1999**, *35*, 4361−4367.
(37) Campanile, R.; Scardapane, E.; Forente, A.; Granata, C.; Germano, R.; Di Girolamo, R.; Minopoli, A.; Velotta, R.; Della Ventura, B.; Iannotti, V. Core-Shell Magnetic Nanoparticles for Highly Sensitive Magnetoelastic Immunosensor. *Nanomaterials* **2020**, *10*, 1526.
(38) Minopoli, A.; Sakač, N.; Lenyk, B.; Campanile, R.; Mayer, D.; Offenhäusser, A.; Velotta, R.; Della Ventura, B. LSPR-Based Colorimetric Immunosensor for Rapid and Sensitive 17β-Estradiol Detection in Tap Water. *Sens. Actuators, B* **2020**, *308*, 127699.
(39) Germano, J.; Martins, V.; Cardoso, F.; Almeida, T.; Sousa, L.; Freitas, P.; Piedade, M. A Portable and Autonomous Magnetic Detection Platform for Biosensing. *Sensors* **2009**, *9*, 4119−4137.

https://doi.org/10.1021/acsomega.2c04442
ACS Omega 2022, 7, 36543−36550